Supplemental Information (SI):

Junction Behavior of n-Si Photoanodes Protected by Thin Ni Elucidated from Dual Working Electrode Photoelectrochemistry

Forrest A. L. Laskowski, Michael R. Nellist, Radhakrishnan Venkatkarthick, and Shannon W. Boettcher

Section S1

The electrical conductivity through the photoelectrochemical (PEC) activated Ni film is largely dependent on the state of the near-solution Ni species. If the surface Ni is in the $Ni(OH)_2$ phase it will behave as an insulator and impede charge transfer. When the catalyst is oxidized to NiOOH, it exhibits much higher conductivity.[1-3] The electrical junction behavior of the composite dual working electrode (DWE) is dependent on what state the Ni is in prior to performing the Au thermal deposition to form the WE_2 contact.

A significant concern in depositing 10 nm of Au on 3 and 5 nm Ni films is the development of direct n-Si | Au shorting. To evaluate this concern, we produced DWE photoanodes wherein the redox active Ni is isolated as $Ni(OH)_2$ prior to Au evaporation. Devices created in this manner can be evaluated for shorting by examining the dark ex-situ J-V characteristics before and after $Ni(OH)_2$ solution oxidation (Figure S1). Without n-Si | Au shorting, the J-V characteristics exhibit poor conductivity which becomes rectifying only once the $Ni(OH)_2$ is electrochemically oxidized to NiOOH. Devices were re-reduced after performing in-situ DWE experiments; these J-V characteristics exhibit good agreement with the initial film which indicates WE_2 stability and sustained lack of shorting. Such "short-free" devices are suitable for further interface analysis.

We note that devices where the Ni is electrochemically oxidized to NiOOH, directly prior to Au depositions, tend to exhibit electrical conductivity despite electrochemical re-reduction (to $Ni(OH)_2$). We speculate that this is caused by small regions of previously redox-active NiOOH being isolated from solution by the thin gold layer. In effect, these regions of Ni are never able to fully re-reduce and thus remain conductive despite the majority of the film being converted to $Ni(OH)_2$. Electrodes produced in this manner are useful in that the junction photovoltage can be sensed at all relevant potentials through WE_2 (discussed more below).

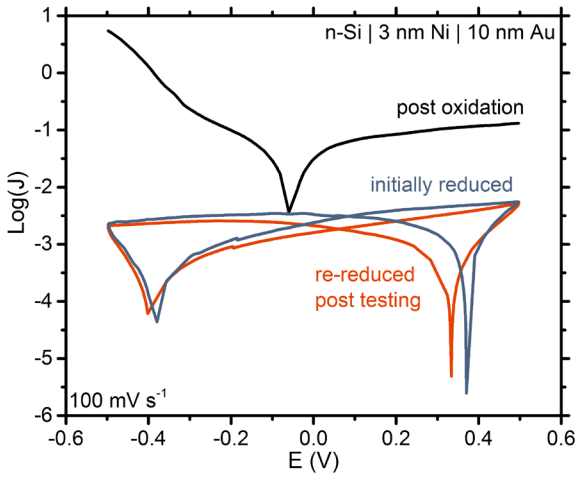

Figure S1. Dark, *ex-situ* JV characteristics for a DWE photoanode with $Ni(OH)_2$ isolation. Catalyst films were isolated as $Ni(OH)_2$ by supplying a reducing potential for 10 min (200 mV cathodic of the reduction peak potential) and to NiOOH by supplying an oxidizing potential for 10 min (200 mV anodic of the oxidation peak potential).

Section S2

To examine electrode activity as a function of (long-term) cycling we photo-deposited additional Ni before evaporation of the Au WE_2. This improved the cycling longevity of the DWE electrode. Such photodeposition of sacrificial Ni is also useful in that it consistently prevents n-Si | Au shorting (which is often observed for the thinner layers). We examine the 5 nm devices because they exhibit an intermediate photovoltage enhancement relative to the 3 and 20 nm devices. During a typical experiment, WE_1 was cycled 49 times through the oxidation and reduction peak without significantly entering the OER region. On the 50th cycle a more extended CV was swept to include the OER region and then WE_2 was cycled once to examine the catalyst activity independent of the semiconductor. After 250 cycles it becomes apparent that WE_2 losses significant contact with the catalyst. This conclusion is consistent with the diminishing redox peaks, likely indicating the dissolution or detachment of sacrificial catalyst.

Figure S2 expands on the data in Figure 3 of the text, and demonstrates the continued effects of this process on both working electrodes. Results show that OER onset significantly improves over 250 cycles when measured from WE_1 but only improves over the first 50 cycles when measured from WE_2. Additionally, the improvement onset potential measured through WE_2 (i.e. catalyst) is ~100 mV while that measured through WE_1 (i.e. semiconductor ohmic contact) is ~400 mV.

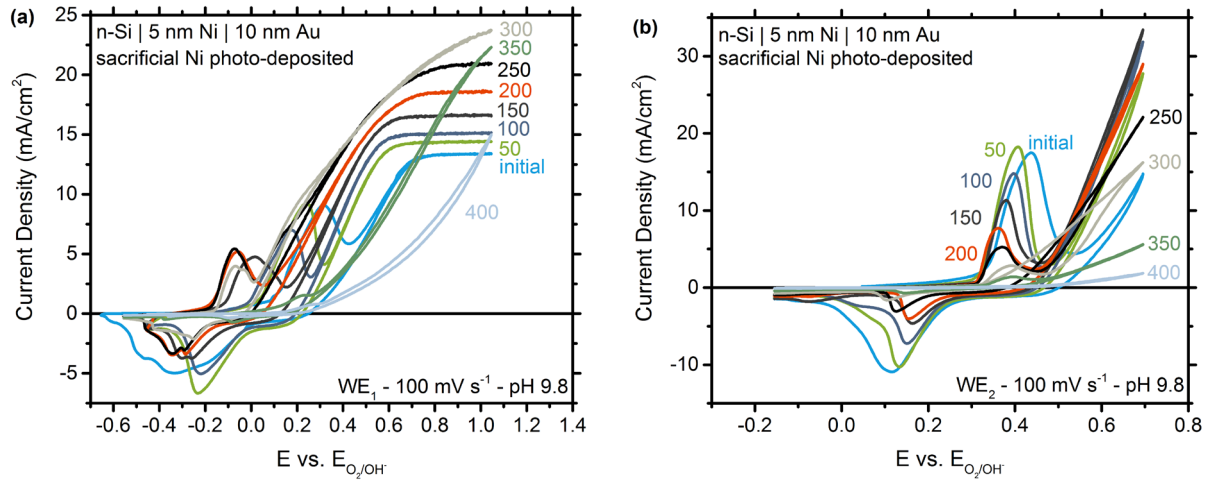

Figure S2. (a) Illuminated cycling experiments through WE_1 on n-Si | 5 nm Ni | 10 nm Au DWE photoanodes. **(b)** Illuminated cycling experiments through WE_2 on n-Si | 5 nm Ni | 10 nm Au DWE photoanodes. Same device as Figure S2a. Both experiments were performed under 100 mW cm^{-2} of AM1.5G solar simulation in a pH 9.8 K-borate buffer.

Because sacrificial catalyst loss is apparent during cycling experiments we controlled for this effect by intentionally "pinning" the junction. To accomplish this a 10 nm Au interlayer was deposited between the n-Si and 5 nm Ni layer. CV experiments were conducted in an identical manner to those in Figure S2. Sacrificial Ni loss was also noticed in this instance but no change in the illuminated OER onset was seen when measured through WE_1. Additionally, the redox peak locations remained largely unaffected by continued cycling, when measured through both WE_1 and WE_2. Whereas in the n-Si | 5 nm Ni junction the redox peaks moved mostly in step with the OER onset increases, when measured through WE_1. This data is consistent with the expected behavior of the buried n-Si | Au junction and shows that the cathodic shifts in photocurrent onset are produced specifically by changes to the n-Si | Ni junction.

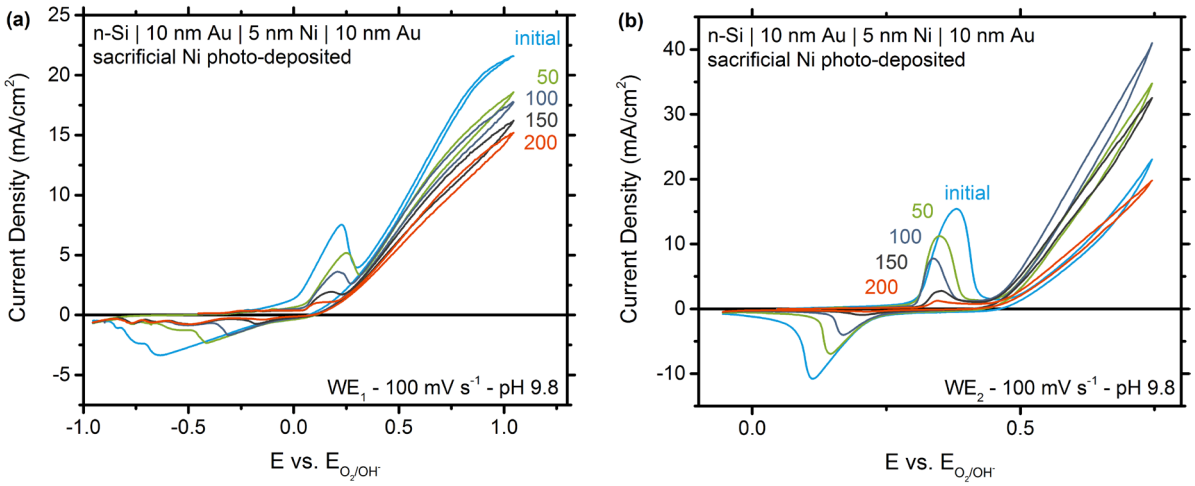

Figure S3. (a) Illuminated cycling experiments through WE_1 on n-Si | 10 nm Au | 5 nm Ni | 10 nm Au DWE photoanodes. **(b)** Illuminated cycling experiments through WE_2 on n-Si | 10 nm Au | 5 nm Ni | 10 nm Au DWE photoanodes. Same device as Figure S3a. Both experiments were performed under 100 mW cm^{-2} of AM1.5G solar simulation in a pH 9.8 K-borate buffer.

Section S3

Thermal evaporation of ~2 nm Ni on n-Si results in photoanodes which decay back to bare n-Si response within ~20 CVs (Figure S4). Limited lifetime is attributed to passivation via holes in the thermally evaporated film and oxidation of the underlying Si surface.

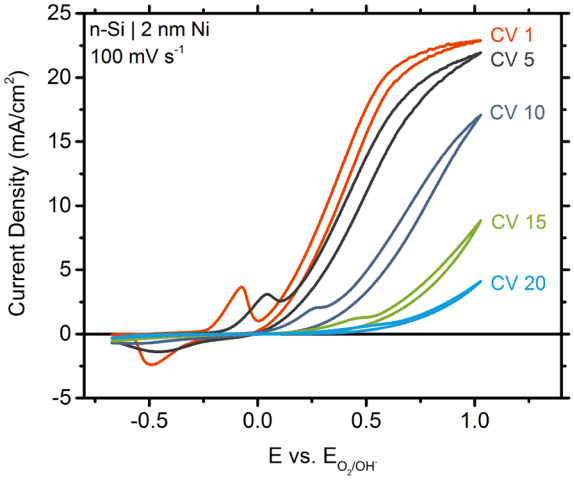

Figure S4. Illuminated degradation of an n-Si photoanode protected with 2 nm metallic Ni. The data was collected under 100 mW cm^{-2} of solar simulation in a pH 9.8 K-borate buffer.

Similarly, cathodic electrochemical deposition of $Ni(OH)_2$, accomplished by maintaining a current density of -0.1 mA cm^{-2} for 10 min in a 0.1 M, pH 7 $NiSO_4$ solution, fail to protect photoanodes at all due to the electrolyte permeability of the catalyst layer (Figure S5). Deposition was sufficiently thick as to be visible by eye.

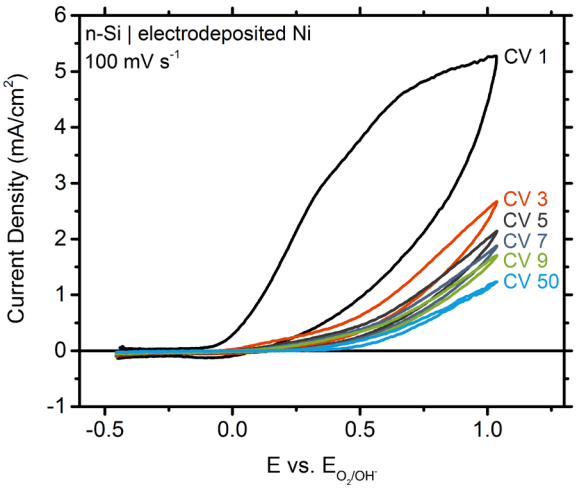

Figure S5. Illuminated degradation of an n-Si photoanode protected with electrochemically deposited Ni. The voltammetry presented shows initial limited photoelectrode performance which degrades rapidly within ~10 cycles. Electrolyte permeable electrodeposited Ni (oxy)hydroxide cannot protect the Si surface. The data was collected under 100 mW cm^{-2} of solar simulation in a pH 9.8 K-borate buffer.

Section S4

Dark linear sweep voltammagrams (LSVs) on control devices (i.e. with direct Au|Si Schottky contact) exhibited the expected behavior for a buried Schottky junction. When normalized to the junction voltage ($E_{sem} - E_{cat}$) the reverse saturation current remained invariant despite stepping the potential at WE_2 through a 500 mV range. In the forward bias regime (negative voltage in Figure S6), when normalized to the junction voltage, curves also collapsed upon each other at all WE_2 potentials. The devices display rectifying behavior, consistent with well-established Schottky diode theory.[4]

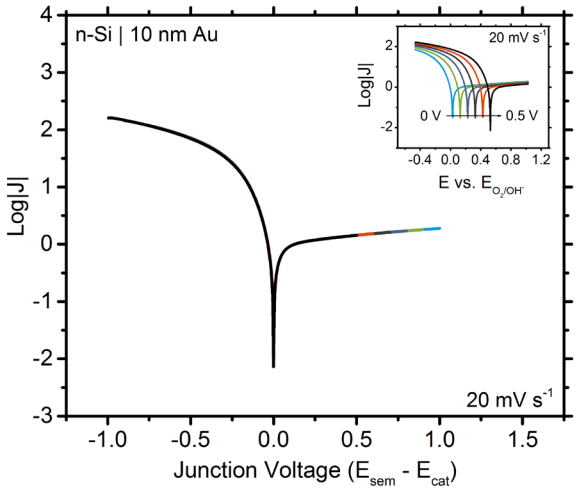

Figure S6. Dark in-situ LSV characteristics for an intentionally buried n-Si | Au junction. Results are normalized to the junction voltage to examine reverse saturation current – a function of barrier height. The data was collected in a pH 9.5 K-borate buffer.

For DWE junction experiments the chemical state of the Ni during deposition of the secondary Au working electrode is an important consideration. The porous Au can either be deposited on surface Ni isolated as NiOOH or as $Ni(OH)_2$. Isolation in the $Ni(OH)_2$ state is useful in that it allows for identification of direct shorting from the Au to the n-Si (discussed above). However, $Ni(OH)_2$ is insulating and will produce a switching behavior in the DWE measurements when oxidized to conductive NiOOH. Isolation in the NiOOH phase eliminates the switching behavior, but n-Si | Au shorting cannot be identified. Both situations are discussed in SI section S1.

To understand better the interface character, we reproduced the DWE experiments with the Ni isolated in the NiOOH phase. Results are then compared to control devices wherein the junction is intentionally pinned; that is, where 10 nm of Au is thermally evaporated before Ni evaporation (Figure S6). The control devices behave as expected for a buried junction; rectifying behavior is exhibited and each curve is nearly identical when normalized to the junction voltage. For DWE photoanodes where the Ni is isolated as NiOOH prior to gold evaporation, the LSVs depict buried junction behavior with a substantially reduced conductivity switch effect between $Ni(OH)_2$ and NiOOH (Figure S7). In both the devices with 3 nm and 5 nm of Ni, the forward bias region is effected by the in-situ transition from $Ni(OH)_2$ to NiOOH. In each case increases in conductivity appear to modestly enhance the current response. Interestingly this effect is more pronounced on the 3 nm Ni protected photoanodes perhaps as a result of fewer NiOOH regions protected by Au. However, examination of the reverse bias region in each case reveals an invariant current response, which is an indication of an invariant barrier height as the potential of the catalyst layer is changed. *The data further supports our hypothesis that protected Si photoanodes in the size regimes explored exhibit buried-junction behavior.*

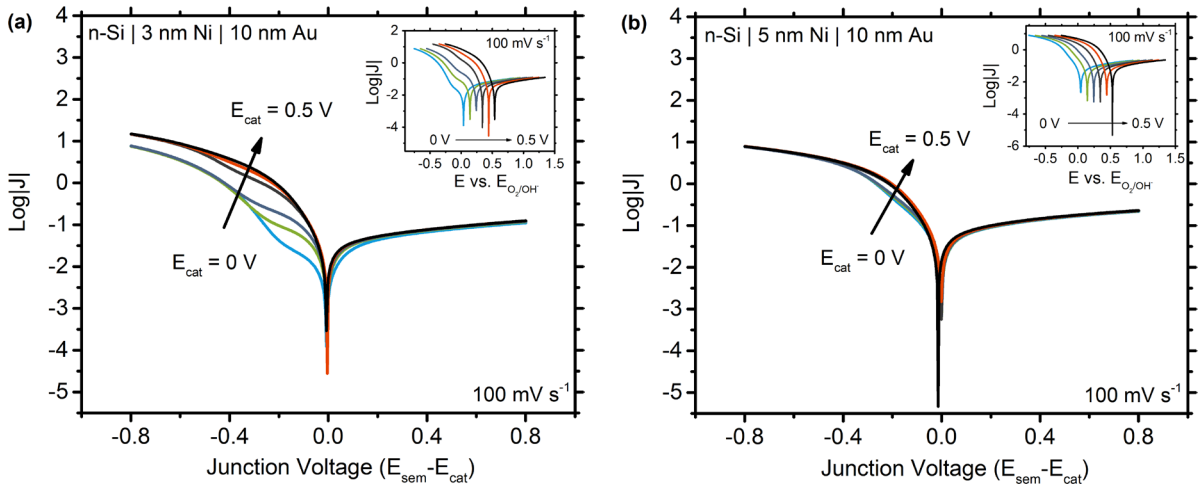

Figure S7. (a) Dark in-situ LSV characteristics for a DWE n-Si | 3 nm Ni | Au junction. In these devices the Au layer was deposited after isolating the Ni in the conductive NiOOH form. **(b)** Dark in-situ LSV characteristics for a DWE n-Si | 5 nm Ni | Au junction. For both data sets E_{cat} is varied via WE_2 in steps of 100 mV through the entire Ni redox region, while current voltage curves across the interface are collected for each E_{cat} by sweeping E_{sem} (WE_1). The data was collected in a pH 9.5 K-borate buffer.

Section S5

To better distinguish the Ni redox peak from the OER region, slower LSVs at 10 mV s^{-1} were collected before and after Fe incorporation. The offset between the two is ~ 99 mV at 2.5 mA/cm^2, consistent with the ~100 mV shift measured through WE_2 at 100 mV s^{-1}.

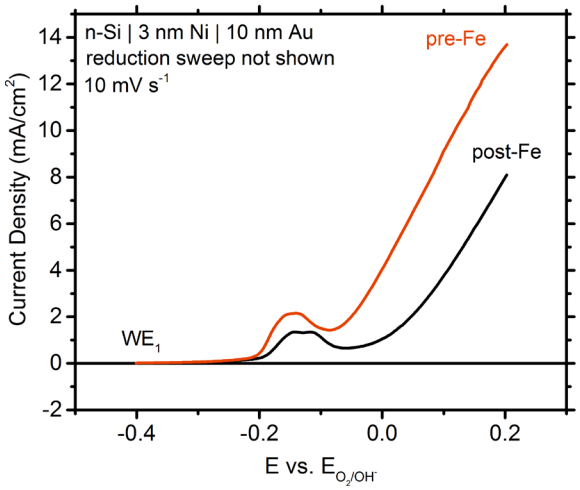

Figure S8. Illuminated 10 mV s^{-1} LSVs collected through WE_1 before and after Fe incorporation. Results are similar to 100 mV s^{-1} LSVs but better resolve the redox peak and OER onset. The data was collected under 100 mW cm^{-2} of solar simulation in a pH 9.8 K-borate buffer.

Section S6

XPS was used to identify the elemental composition and oxidation states of n-Si protected with 3 nm of Ni before and after electrochemical cycling. The raw data was shifted such that the adventitious carbon 1s peak was centered at a binding energy of 284.8 eV. A depth profile, via Ar ion sputtering (2 keV, 3 μA), was conducted in 5 s increments to determine compositional changes as a function of depth. For the *post-cycled* electrodes (Figure S9) XPS data shows that the surface is primarily composed of nominally Ni hydroxide/oxyhydroxide (Figure S9a). However, the depth profile indicates that residual metallic Ni persists under this layer and becomes the dominant Ni species after 20 s of Ar ion sputtering. Interestingly, this layer later gives way to an XPS spectrum consistent with NiSi, demonstrating direct contact between Si and Ni, even in the electrochemically cycled device. The Si regional spectra (Figure S9b) illustrates that the SiO_2 layer has been milled through after ~75s of cumulative Ar ion sputtering.

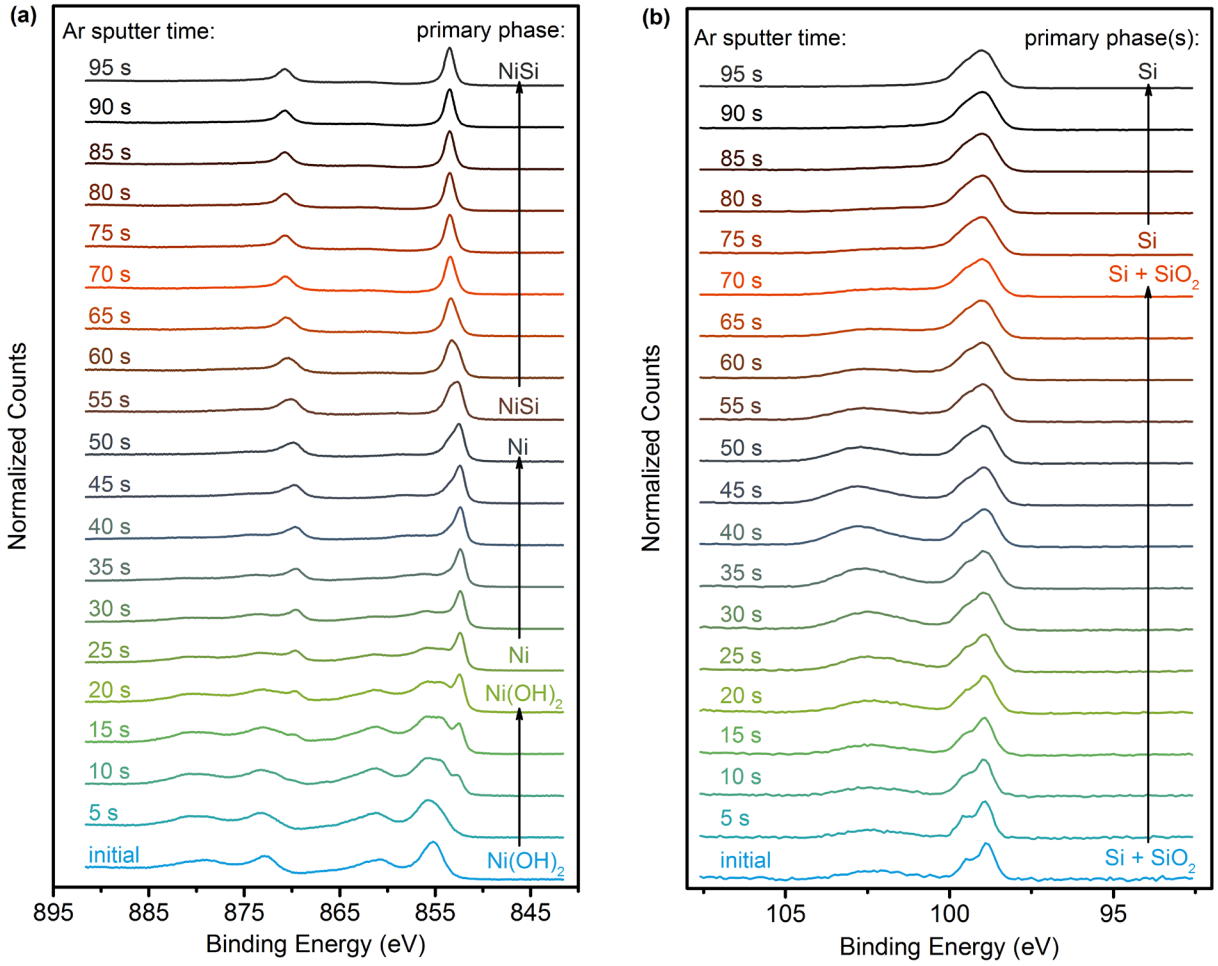

Figure S9. XPS spectra of n-Si protected with 3 nm of Ni after electrochemical cycling. (a) The Ni region of the XPS profile exhibits a transition from $Ni(OH)_2$ to Ni to NiSi. (b) The Si region of the XPS profile exhibits increased SiO_2 character for the first 35 s before it completely diminishes after 75 s. This is consistent with a depth profile which has passed through a Si oxide layer consisting of the native oxide and any oxidized regions formed during electrochemical cycling.

Peaks were identified using the ThermoScientific Avantage 4.75 software, comparisons to Mullins et al. monochromated Kα spectra, and comparisons to the NIST XPS Database 20, version 4.1 binding energies.[5,6] Select spectra are taken from Figure S9a above and labeled in more detail below (Figure S10).

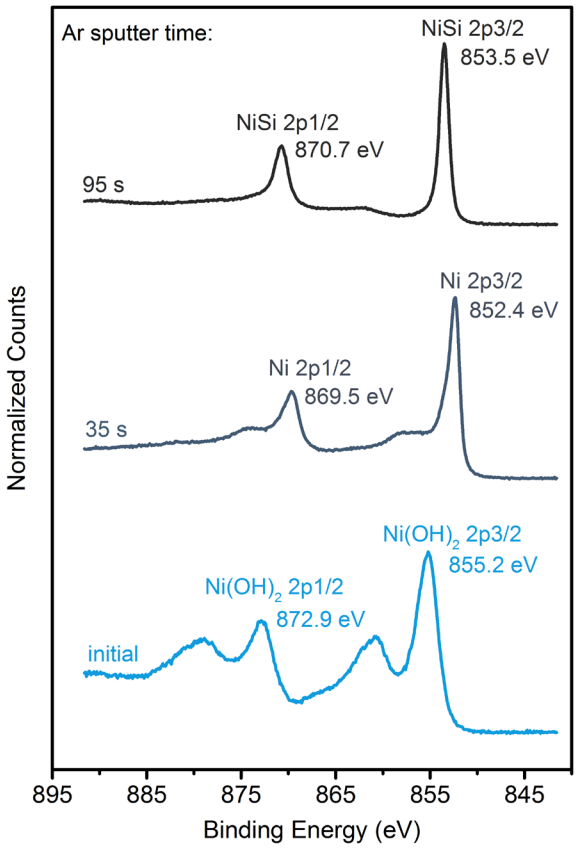

Figure S10. Select sputter times selected from Figure S9a to identify key peak positions. Peak locations and general shapes were compared to monochromated Kα spectra from Mullins et al. and the NIST XPS database.

As-deposited samples not subject to electrochemical cycling exhibit a metallic Ni peak before depth profiling (Figure S11).

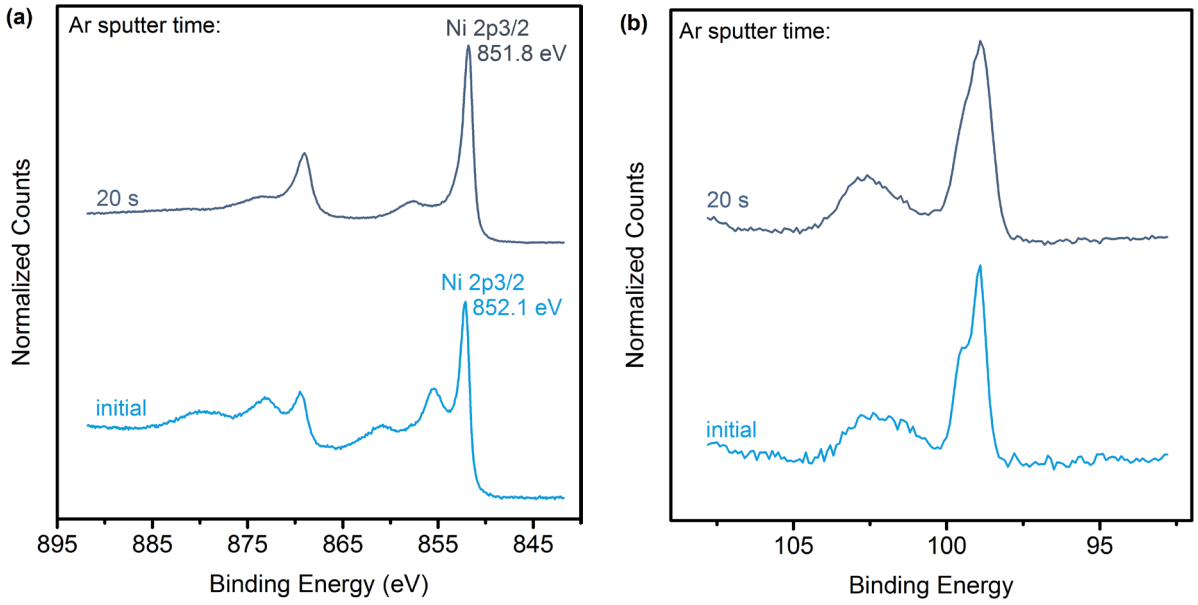

Figure S11. XPS spectra at select sputter times for control samples of n-Si protected with 3 nm of Ni without electrochemical cycling: (a) the regional Ni spectra and (b) the regional Si spectra.

Reduction of $Ni(OH)_2$ to metallic Ni by Ar ion sputtering has been documented in other systems.[7] A control sample, fabricated by electrodepositing $Ni(OH)_2$ onto an Au/Ti-coated glass slide, was used to examine the extent of $Ni(OH)_2$ reduction from this process (Figure S12). During the first three sputter steps (identical conditions as above) the Ni regional spectrum changes significantly as a shoulder grows into the Ni 2p 3/2 peak – consistent with the presence of metallic Ni. However, for subsequent sputter steps the spectrum remains largely unchanged – consistent with establishment of a steady state ratio of metallic Ni to $Ni(OH)_2$ as the Ar ion milling removes material. In the Ni-protected n-Si samples, analyzed after electrochemical cycling, a transition to purely metallic Ni is observed - this indicates the presence of metallic Ni before sputtering. *The metallic Ni observed in the cylced photoelectrodes is thus not an artifact from Ar ion sputtering.*

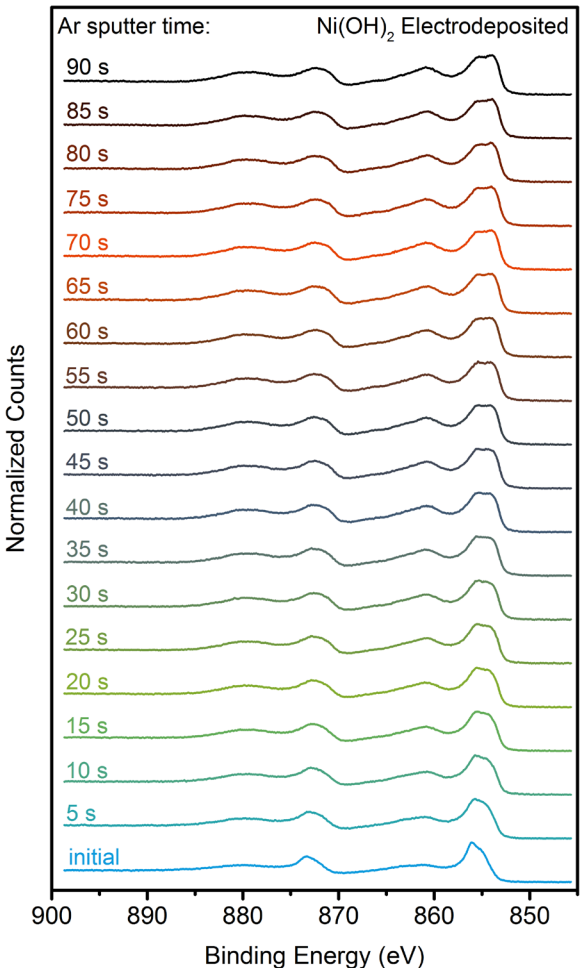

Figure S12. XPS spectra of $Ni(OH)_2$ electrodeposited (-2 mA for 60 s in a 0.1 $Ni(NO_3)_2$ solution) onto Au, after electrochemical cycling. The Ni region of XPS profile shows the conversion of some $Ni(OH)_2$ to metallic Ni and the establishment of a steady state ratio between the two species.

Section S7

Non-saturated photocurrent and cleaning procedure dependence. The majority (95%+) of electrodes fabricated with the simple IPA cleaning procedure exhibit non-constant photocurrent in the saturated regime. As discussed in the main text, this behavior can be attributed to the pinch-off effect, arising from a spatially heterogenous junction. Interestingly, altering the cleaning procedure by adding a 1 min HF buffered oxide etch (BOE) followed by a 10 min Radio Corporation of America (RCA) SC-2 clean, produces constant photocurrent in the saturated regime. However, this change in photocurrent behavior is accompanied by a significantly diminished photocurrent onset and reduced redox peak integration (Figure S13). It appears that the altered cleaning procedure leads to a more-conformal coating which then reduces the electrolyte's ability to permeate to the semiconductor | catalyst junction. Lack of permeation is apparent from the reduced redox integration. In turn, spatial barrier height heterogeneity decreases (as indicated by the saturated photocurrent profile at sufficiently anodic potential) and better photocurrent onset potentials are precluded because the pinch-off effect is no longer a dominant process.

This view is supported by AFM analysis which depicts smoother films, post-Ni deposition, when the altered cleaning procedure is used. Additionally, the photocurrent onset of the 3 nm devices deposited with the altered cleaning procedure compares favorably with the devices protected by 20 nm of Ni in Figure 2 of the main text. *The data further supports our hypothesis that sufficient spatial barrier height heterogeneity allows the interface to generate larger photovoltages.*

A further consideration in employing the altered cleaning procedure is the possible alleviation of shallow defect states responsible for Fermi level pinning (as discussed in the main paper). Growth of a more conformal and dense SiO_2 layer, via the RCA SC-2 clean, may accomplish this goal and result in a larger photovoltage. However, if this effect is present it is ultimately obscured by the apparent photovoltage loss associated with precluding development of spatially heterogenous barrier heights.

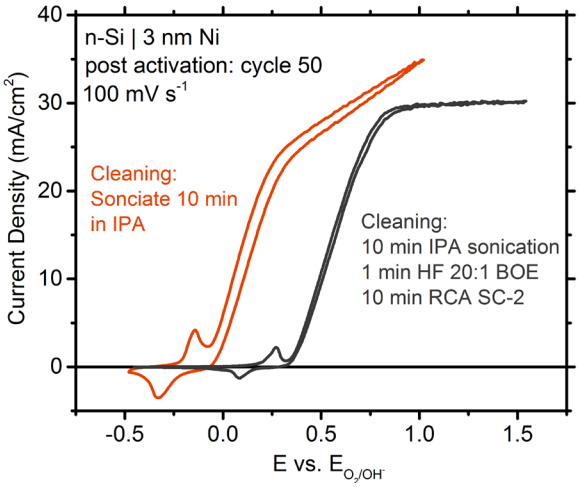

Figure S13. Comparison of illuminated CVs for n-Si protected with 3 nm Ni after activation protocol. The more rigorous cleaning procedure (black curve) results in a decreased onset potential and diminished redox integration. The data was collected under 100 mW cm^{-2} of solar simulation in a pH 9.8 K-borate buffer.

Section S8

Material characterization with AFM reveals a relatively smooth surface for electrodes imaged directly after 3 nm Ni evaporation (Figure S14a). We identify the surface speckles as adventitious particulate contamination incorporated during the fabrication process. This view is supported by the lack of these defects in films where additional cleaning procedures were used (1 min 20:1 HF BOE and 10 min RCA SC2) and by the quick disintegration of these features during SEM imaging. After the standard PEC activation protocol, films roughen and develop island features > 100 nm in diameter and particulate contamination generally persists (Figure S14b). This is consistent with oxidation of the majority of the film to Ni (oxy)hydroxide.

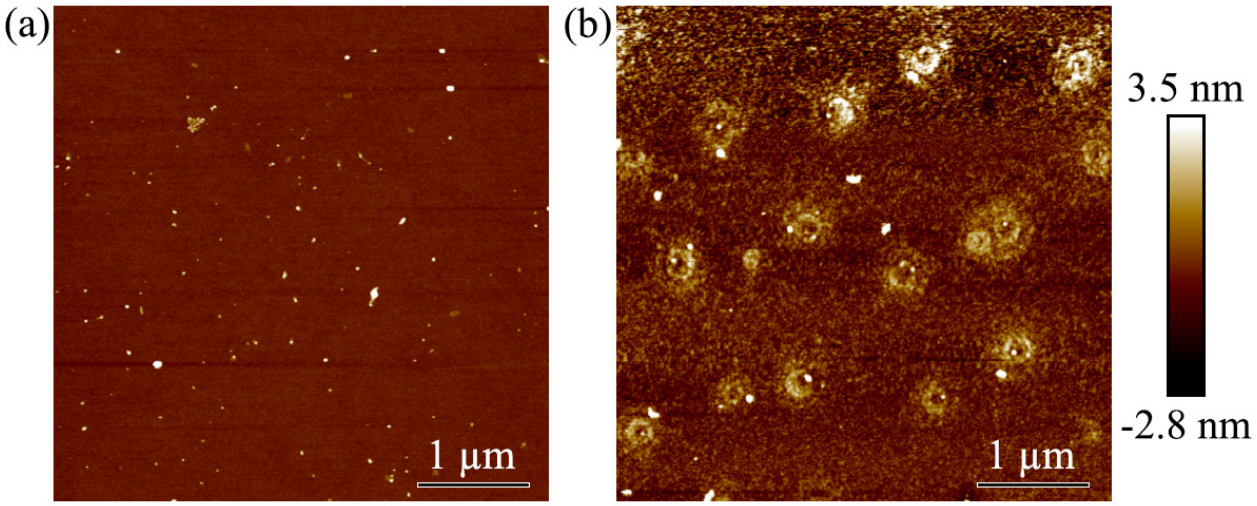

Figure S14. AFM images of n-Si protected with 3 nm of Ni **(a)** before electrochemical cycling and **(b)** after electrochemical cycling.

Imaging the films after the activation protocol with SEM also reveals the island features (Figure S15). We hypothesize that incomplete Ni protection, caused by the oxidation to Ni (oxy)hydroxides, leads to rapid passivation (SiO_2 growth) in most areas of the film, consistent with the XPS spectra shown earlier.

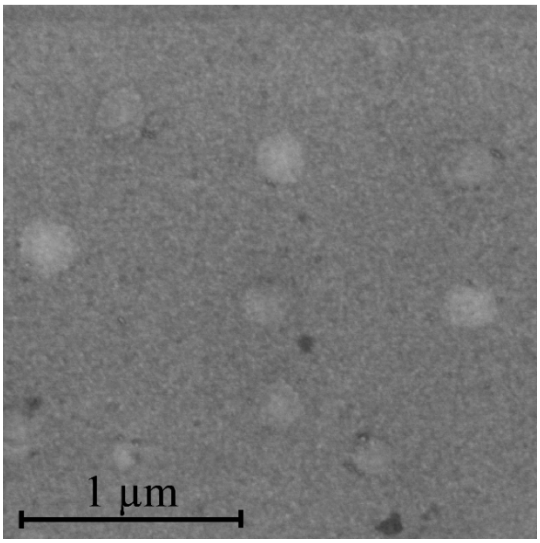

Figure S15. SEM image of n-Si protected with 3 nm of Ni after electrochemical cycling.

Citations

1. A. M. Smith, L. Trotochaud, M. S. Burke, and S. W. Boettcher, *Chem. Commun.*, 2015, **51**, 5261–5263.
2. M. S. Burke, L. J. Enman, A. S. Batchellor, S. Zou, and S. W. Boettcher, *Chem. Mater.*, 2015, **27**, 7549–7558.
3. L. Trotochaud, S. L. Young, J. K. Ranney, and S. W. Boettcher, *J. Am. Chem. Soc.*, 2014, **136**, 6744–6753.
4. S. M. Sze, *Semiconductor Devices: Physics and Technology*, 2008.
5. A. Kraut, *NIST X-ray Photoelectron Spectroscopy Database 20. Version 4.1, 2012*.
6. J. F. Moulder, W. F. Stickle, P. E. Sobol, and K. D. Bomben, *Standard Spectra for Identification and Interpretation of XPS Data*, 1992.
7. K. S. Kim and N. Winograd, *Surface Science*, 1974, **43**, 625–643.